

## NAR Breakthrough Article

# 3.9 Å structure of the nucleosome core particle determined by phase-plate cryo-EM

Eugene Y.D. Chua<sup>1</sup>, Vinod K. Vogirala<sup>1</sup>, Oviya Inian<sup>1</sup>, Andrew S.W. Wong<sup>2</sup>,  
Lars Nordenskiöld<sup>1</sup>, Juergen M. Plitzko<sup>3</sup>, Radostin Danev<sup>3</sup> and Sara Sandin<sup>1,2,\*</sup>

<sup>1</sup>School of Biological Sciences, Nanyang Technological University, 637551, Singapore, <sup>2</sup>NTU Institute of Structural Biology, Nanyang Technological University, 639798, Singapore and <sup>3</sup>Department of Molecular Structural Biology, Max Planck Institute of Biochemistry, Martinsried 82152, Germany

Received April 22, 2016; Revised July 08, 2016; Accepted August 02, 2016

### ABSTRACT

**The Volta phase plate is a recently developed electron cryo-microscopy (cryo-EM) device that enables contrast enhancement of biological samples. Here we have evaluated the potential of combining phase-plate imaging and single particle analysis to determine the structure of a small protein–DNA complex. To test the method, we made use of a 200 kDa Nucleosome Core Particle (NCP) reconstituted with 601 DNA for which a high-resolution X-ray crystal structure is known. We find that the phase plate provides a significant contrast enhancement that permits individual NCPs and DNA to be clearly identified in amorphous ice. The refined structure from 26,060 particles has an overall resolution of 3.9 Å and the density map exhibits structural features consistent with the estimated resolution, including clear density for amino acid side chains and DNA features such as the phosphate backbone. Our results demonstrate that phase-plate cryo-EM promises to become an important method to determine novel near-atomic resolution structures of small and challenging samples, such as nucleosomes in complex with nucleosome-binding factors.**

### INTRODUCTION

Single particle electron cryo-microscopy (cryo-EM) is a powerful technique for structure determination of isolated macromolecular complexes at near-atomic resolution. Several important developments have contributed to the recent ‘resolution revolution’ in cryo-EM, including direct electron detection, correction of beam-induced motion, as well as

improved classification and 3D reconstruction procedures (1–3). The technique is particularly suitable for structure determination of large and flexible macromolecular complexes. Therefore, cryo-EM can potentially be used for high-resolution structural analysis of nucleosomes reconstituted in complex with chromatin-binding factors for which we have no or limited structural information. However, the nucleosome is a challenging target compared to proteins routinely analysed in cryo-EM due to several reasons. First, nucleosomes are small (200 kDa), which can be problematic to detect (particle picking), align and structurally analyze (4). Second, excess DNA is required to prevent chromatin aggregation, resulting in a reduced contrast difference between particles and the surrounding ice. Third, certain orientations of the nucleosomes are difficult to detect, even in micrographs recorded at high defocus, resulting in systematic loss of data and resolution. Therefore, interpretation of EM density and particle picking is problematic.

Biological samples are weak-phase and radiation-sensitive objects (2,5). The most common approach to generate contrast in cryo-EM is to record images out of focus (defocus by 1–3 μm), which is referred to as bright field phase contrast EM. An alternative technique is to utilize phase plate EM (6). The principle is similar to phase contrast imaging in light microscopy with a Zernike phase plate. In a Transmission Electron Microscope (TEM), the phase plate is positioned in the back focal plane of the objective lens, introducing a phase shift between the scattered and un-scattered electron waves. The advantage of phase plate imaging over bright field phase contrast imaging is that it maintains low-resolution frequencies without zeros or phase-flipping effects in the Contrast Transfer Function (CTF). Therefore, small particles can be detected and analysed without CTF correction. This was demonstrated in a recent phase-plate cryo-EM recon-

\*To whom correspondence should be addressed. Tel: +65 65923672; Fax: +65 67913856; Email: ssandin@ntu.edu.sg

struction of the peroxiredoxin-3 dodecamers (257 kDa) (7), obtained to a resolution of 4.4 Å, sufficient to resolve individual beta-strands but not amino acid side chains.

Here, we have used the 200 kDa Nucleosome Core Particle (NCP) as a test specimen for imaging protein–DNA complexes by phase-plate cryo-EM. The NCP is a sub-complex of the nucleosome, the repeating unit of eukaryotic chromatin. It consists of core histones (two copies each of histone proteins H2A, H2B, H3 and H4) and 145 base pairs of DNA (8). Early EM and X-ray crystallographic analysis of nucleosomes revealed that DNA is wrapped around the core histones in left-handed superhelical turns, forming a disk shaped particle 101×57 Å in diameter (9–11). Subsequent high-resolution X-ray crystallographic analysis at 2.8 Å (12) and 1.9 Å (13) revealed, in atomic detail, the organization of core histone proteins and DNA. We show here that cryo-EM images recorded with a Volta phase plate (14) can be used to reconstruct a 3.9 Å map of the NCP, to which an atomic model can be built.

## MATERIALS AND METHODS

NCPs were reconstituted as described previously (15) using recombinant *Xenopus laevis* histones and 145 base pairs of 601 DNA. Briefly, histones and DNA were mixed in 20 mM HEPES pH 7.5, 1 mM EDTA, 1 mM DTT and 2 M KCl, and then dialyzed against a gradient of decreasing salt at room temperature over 16 h. The final dialysis was carried out using a no-salt buffer. The reconstitution was analysed on a 6% native polyacrylamide gel, after which the NCP sample was concentrated using an Amicon 10 kDa cut-off concentrator (Supplementary Figure S1). Grids were prepared using freshly glow-discharged holey carbon grids (Quantifoil R2/2 and R1/4), 3–4 µl of sample per grid, 3–4 s blotting time, liquid ethane/propane and a Vitrobot (FEI) plunge-freezer. The concentration of NCP used was 1.0 mg/ml for R2/2 grids and 2.5 mg/ml for R1/4 grids.

Electron micrographs shown in Supplementary Figures S2 and S3 were recorded on a Tecnai Arctica (FEI) at 200 kV with a Falcon2 direct electron detector (FEI). Electron micrographs shown in Figure 1 were recorded on Titan Krios (FEI) at 300 kV with a K2 Summit (Gatan) direct electron detector in counting mode. The Volta phase plate (FEI) was used on both microscopes. Data was collected in nanoprobe mode and parallel illumination. The Krios microscope settings, pixel size and image processing statistics used for high-resolution refinements are listed in Table 1. Focusing and conditioning of the phase plate was done manually on the Arctica (using stage shift to move from carbon to exposure regions). Focusing was done automatically on the Krios with SerialEM (16), using multiple focus regions (repeated three times on two sides of the exposure area). The phase plate position and astigmatism were changed and corrected manually on both microscopes. A total of 20–60 images were collected at each phase plate position on the Krios. Bad images, such as images recorded out of focus, were removed by manual inspection. Pixel outliers were removed using the clip function in Imod (17).

Frames were aligned and integrated using the unblurred-movie software (18) without applying dose weighting.

Particles were picked semi-automatically in EMAN2 (19) and then extracted and processed in RELION 1.3 (20). The particles were sorted by 2D and 3D classification, as well as by Z-score, from which the best 26,060 particles were selected for high-resolution 3D refinement. A total of 12,309 particles did not have a high alignment score, which may be due to image quality or structural heterogeneity. The 2D class sums shown in Figure 1B were calculated using particles binned by a factor of 2. The 3D refinement was done without binning to keep high-resolution information. A density map of the NCP, filtered to 80 Å resolution, was used as a starting model and C2 symmetry was applied to the refinement. The data was processed without CTF correction. Particle polishing significantly improved the B-factor (Table 1) and overall appearance of the map. The resolution was estimated using Fourier Shell Correlation (FSC=0.143, gold-standard). A comparison of the FSC curves of the EM map and randomized phases is shown in Figure 2A. The local resolution of the map was determined in ResMap (21). The micrographs shown in Figure 1A and C, and Supplementary Figure S2 were bandpass filtered with ImageJ (22) for clarity. The bandpass filter was set to remove information below 4 Å and above 500 Å. Supplementary Figure S3 shows field views (raw micrographs) without bandpass filtering. The NCP-601 model (PDB ID 3LZ0) was docked into the map and visualized in UCSF Chimera (23). As a final step, the NCP-601 model was refined using phenix.real\_space\_refine (24).

## RESULTS

### Phase-plate cryo-EM analysis of the nucleosome core particle and DNA

To obtain a homogenous and stable NCP sample suitable for high-resolution cryo-EM analysis we made use of a sequence, called Widom 601, that uniquely positions DNA on the histone octamer (25). Recombinant *Xenopus laevis* histones (H2A, H2B, H3 and H4) were used for NCP reconstitution by salt gradient dialysis as described in Materials and Methods. In our experience, excess DNA improves solubility of chromatin and can be beneficial to capture NCPs in ice. To obtain a good particle concentration for cryo-EM, we tested different NCP concentrations and different support grids. We obtained a good particle concentration using either 1.0 mg/ml and R2/2 EM grids, or 2.5 mg/ml and R1/4 EM grids. Next we recorded cryo-EM images of the NCP with and without the Volta phase plate. The phase plate increased contrast of NCPs in ice dramatically (Supplementary Figures S2 and S3). This contrast enhancement was particularly valuable for detecting low-contrast disk views of the NCP. As a control, we repeated the experiment using 601 DNA alone (Supplementary Figure S2C and D). As expected, individual strands with the expected dimensions of double-stranded DNA were observed. We concluded that phase plate imaging provides a marked contrast enhancement of NCPs and free DNA in cryo-EM.

Theoretical and experimental measurements have shown that 300 kV and 20 nm focus accuracy is required for high-resolution single particle analysis with the Volta phase plate, as demonstrated on the 20S proteasome (26). At 200 kV, the phase shift builds up faster resulting in fewer images that

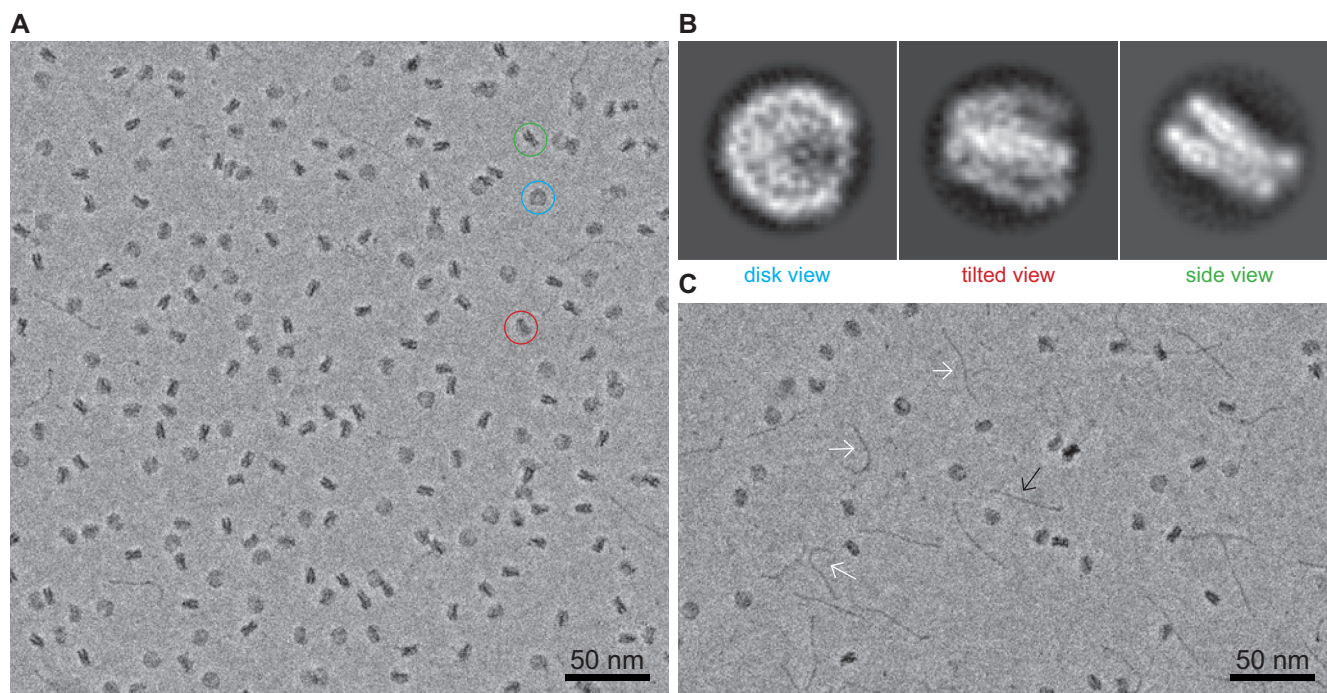


**Figure 1.** Phase-plate cryo-EM analysis of Nucleosome Core Particles (NCPs) in ice. (A and C) Field views of NCP particles recorded with the Volta phase plate. Representative views of the NCP circled in blue (disk view), in red (tilted view) and in green (side view). Arrows indicate excess DNA, in white (bent DNA) and in black (straight DNA). Scale bars are 50 nm. (B) Examples of reference-free 2D class averages showing representative disk, tilted and side views. Mask diameter is 12 nm.

**Table 1.** Data collection and image processing statistics

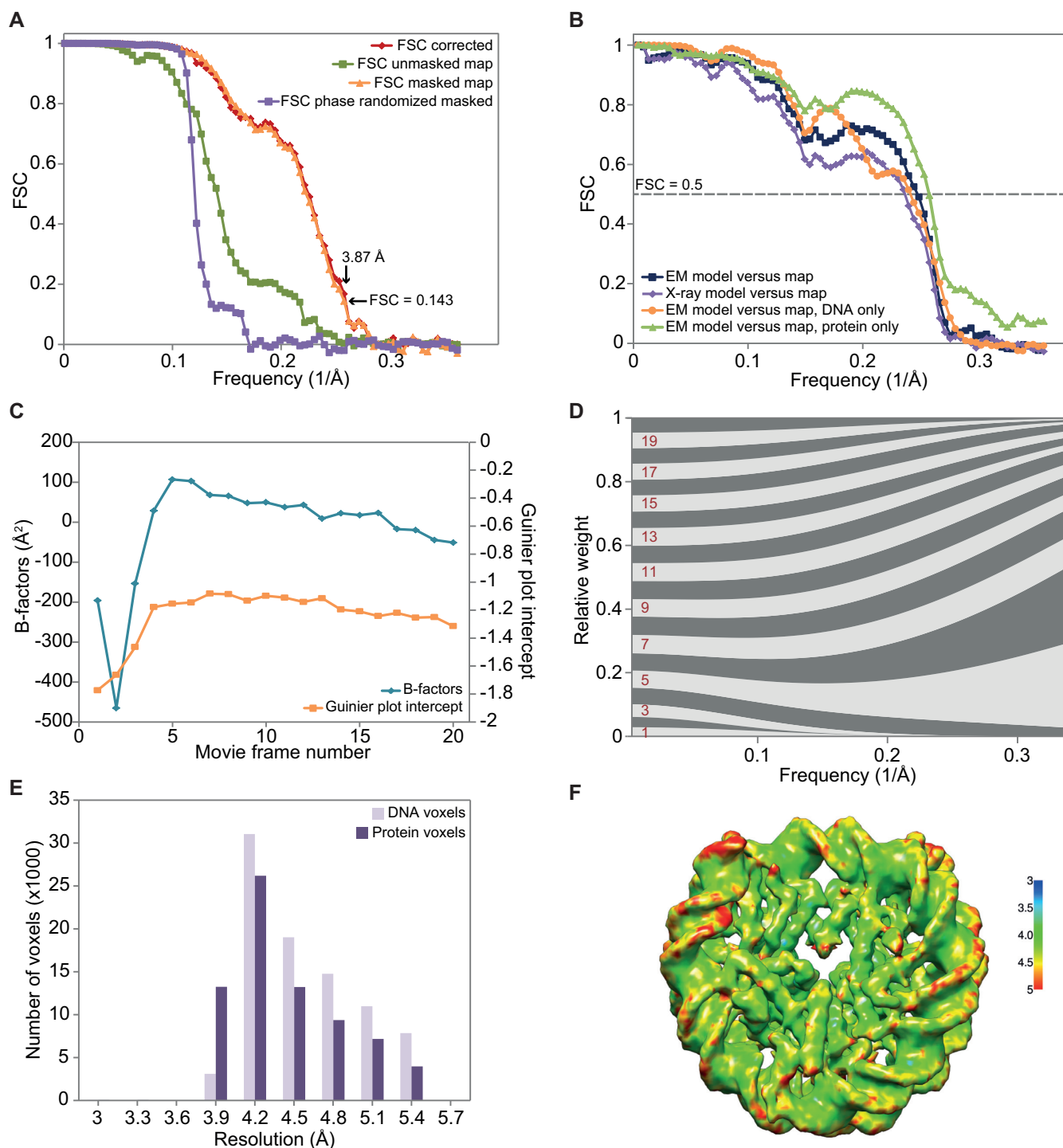
Molecular mass (kDa)	200	Symmetry	C2
Sample support	Quantifoil R1/4	Resolution (Å) Integrated/Movie	4.10/3.87
Microscope	Titan Krios	B-factor (Å <sup>2</sup> ) Integrated/Movie	-132.35/-78.96
Detector	K2	Running average frames/window	7/500
Voltage (kV)	300	Accuracy rotations (°)	1.92
Pixel size/Box size (Å)	1.38/221	Accuracy translations (pix)	0.57
No. movie frames	20	Model-to-map fit (across atoms in volume)	0.78
Exposure time (s)	10	All-atom clash score	8.53
Electron dose (e <sup>-</sup> /Å <sup>2</sup> )	31	Ramachandran plot outliers/allowed/favored (%)	0/5.71/94.29
Micrographs recorded/used	525/445	Rotamer outliers (%) / Cbeta deviations	0/0
Particles picked/used	38,409/26,060	RMSD bond/angle (Å/°)	0.01/0.77

can be recorded per phase plate position. Therefore, we collected a NCP phase plate data set on a 300 kV Krios TEM using multiple focus regions in SerialEM (16) as described in Materials and Methods. A total of 20–60 images were recorded at each phase plate position. A change of phase plate position and correction of astigmatism was carried out manually every 1–2 h. Using this approach, we obtained 525 phase plate images, 445 of which were in focus as judged by visual inspection of images and power spectra.

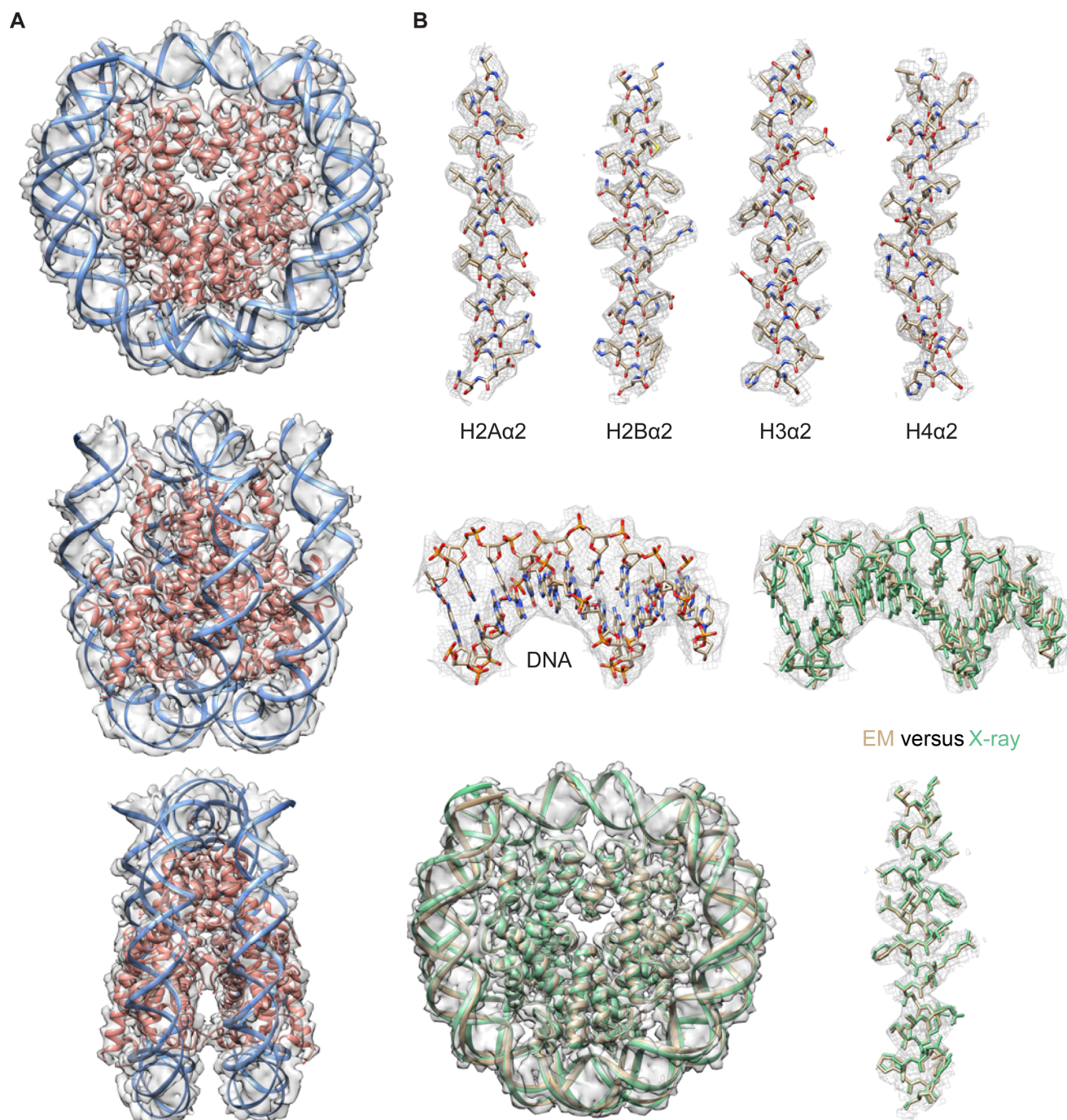
### 3.9 Å structure of the nucleosome core particle

Figure 1A shows a representative phase-plate cryo-EM image recorded in focus, with a good particle distribution and strong contrast of individual NCPs in vitrified ice. NCPs can be clearly recognized in different orientations (representative views encircled in Figure 1A), which we interpret as disk, tilted, and side views, based on structural information of the NCP from previous X-ray crystallographic studies. High-resolution details such as the DNA dyad, major

and minor DNA grooves and histone alpha helices can be seen in the calculated 2D class averages (Figure 1B). Excess DNA can also be clearly identified, which had the appearance of bent or straight DNA strands (highlighted with arrows in Figure 1C). For 3D structure determination, we processed a stack containing 38,409 NCPs by single particle analysis in RELION (20). After 2D and 3D classification, the best 26,060 particles were selected for high-resolution refinement as described in Materials and Methods. Image processing statistics and results are presented in Table 1 and Figure 2. The NCP structure was calculated using C2 symmetry, corresponding to 52,120 asymmetric units, without applying CTF correction. We obtained a resolution of 3.87 Å and a B-factor of -78.96 Å<sup>2</sup>. Next we refined the atomic structure of the NCP-601 (PDB ID 3LZ0), previously determined by X-ray crystallography (27), into our EM map by real space refinement in Phenix (24). The model-to-map correlation was 0.78 (across atoms), and no outliers were detected in the Ramachandran plot (Table 1). We concluded



**Figure 2.** Data processing and map statistics. **(A)** Fourier Shell Correlation (FSC) plots for the EM density map. Arrows indicate 3.9 Å resolution estimate at FSC=0.143. A comparison of the FSC corrected (red), masked (orange), unmasked (green) and phase-randomized (purple) map is shown. **(B)** FSC of the EM map and atomic models derived from the X-ray structure (purple) and the refined model (dark blue) of the NCP, DNA alone (orange) and protein alone (green). **(C)** Per-movie-frame B-factors and Guinier plot intercepts. **(D)** Frequency-dependent weighting of movie frames (frame numbers in maroon). The contributions of early and late frames are down-weighted due to particle movement and beam damage. **(E-F)** Local resolution estimate in ResMap showing that the protein density is better refined as compared to the DNA density (also shown in B).



**Figure 3.** 3.9 Å phase-plate cryo-EM structure of the Nucleosome Core Particle (NCP). (A) Three views of the EM map (surface rendered in grey) and the refined EM model (cartoon representation). The disk view (top) and the tilted view (middle) is related by a 60° rotation about the vertical axis. The disk view (top) and the side view (lower panel) is related by a 90° rotation about the vertical axis. The DNA is shown in blue and histone octamer in pink. (B) Close-up views of histone helices and the DNA dyad. Also shown is a comparison of the EM model (gold) and the X-ray model (green; PDB ID 3LZ0) displaying a similar arrangement of the histone core and small differences in DNA conformations at the entry/exit site of the NCP.

that a data set of less than 40,000 particles was sufficient to obtain a near-atomic structure of the NCP by phase-plate cryo-EM.

Figure 3 shows a gallery of views of the 3.9 Å phase-plate cryo-EM structure together with the refined atomic model. Figure 3A shows the EM density map (surface rendered in grey) with the arrangement of alpha helices in the histone

core (pink) and DNA backbone (blue). Figure 3B contains close-up views of individual histone helices, illustrating that densities for large amino acid side chains can be clearly recognized. The DNA phosphate backbone can also be identified in the EM density map (Figure 3B, middle panel), yet the resolution was insufficient to resolve the separation of individual DNA bases. Figure 2B and E shows a plot of

the local resolution using separate protein and DNA masks. This analysis shows that the protein content of the NCP is better refined than the DNA, indicating that DNA is more flexible than the histone core. Next we compared the phase-plate cryo-EM structure presented here to the previously determined X-ray structure of the NCP-601 (27). Inspection of the protein density shows a remarkable similarity between the two structures (Figure 3B lower panel), including a similar arrangement of the entire histone core. Only small differences in the DNA conformation at the entry and exit sites of the NCPs were detected, which may be due to crystal packing interactions or DNA breathing, whereby the DNA fluctuates spontaneously. As such, we expect the resolution to improve in future studies using larger data sets containing more particles.

## DISCUSSION

The regulation of chromatin is key to the control of gene transcription, DNA replication and eukaryote development. The nucleosome is the basic structural unit of chromatin, yet how proteins interact with the nucleosome is still poorly understood. Clearly, detailed structural information is required to obtain mechanistic insight into how chromatin is regulated. Cryo-EM studies of chromatin, such as nucleosome arrays and chromatin remodelling factors (28–31), have so far been limited to large complexes and intermediate resolution (7.8–25 Å). In contrast, X-ray crystallography has been used for high-resolution structure determination of small chromatin complexes, such as the NCP (9,11–13). There are, however, only a handful of high-resolution structures determined of nucleosomes in complex with nucleosome-binding factors (32). New technological advances in cryo-EM offer the potential to determine high-resolution structures of such challenging and structurally heterogeneous samples.

Here, we applied the recently developed Volta phase plate to determine a 3.9 Å resolution structure of the NCP by single particle cryo-EM. The structure was calculated from micrographs recorded close to focus, using only 26,060 particles (52,120 asymmetric units with C2 symmetry). The structure represents one of three phase-plate cryo-EM structures determined to date. As compared to the 20S proteasome (26) (750 kDa) at 3.2 Å resolution, and the peroxiredoxin-3 dodecamers (7) (257 kDa) at 4.4 Å resolution, the NCP is smaller and has lower symmetry.

We show that phase-plate imaging provides a number of advantages over conventional bright field EM, and so may become an important tool in structural biology. For example, the phase plate greatly improves detection and interpretation of structure and orientation of small particles in ice. Importantly, disk view orientations of the NCP could be detected, resulting in an even distribution of views and unbiased dataset. In addition, nucleosomes can clearly be distinguished from excess DNA. Picking particles and evaluating if the sample preparation is good, containing homogeneous complexes, is not straightforward in bright field EM. Typically, this can only be appreciated after processing large data sets applying class averaging and CTF correction. With phase-plate cryo-EM, there is no question as to what is a nucleosome and what is not. This reduces the risk of inter-

preting noise or DNA as a particle and enables faster image analysis and structure determination.

This represents, to our knowledge, the highest resolution cryo-EM structure of a chromatin complex determined to date. Our future aim is to improve the resolution by collecting larger data sets and include more particles in the refinement procedure. However, software developments, such as improved alignment procedures and change of phase plate position, will be required to fully integrate the Volta phase plate with automatic data collection software for high-throughput analysis. Obtaining high-resolution cryo-EM structures of chromatin complexes will allow us to observe this important biological object in vitreous ice where external forces caused by crystal packing do not interfere with their structure and dynamics. Furthermore, the improved contrast due to the phase plate results in clearly visible naked DNA molecules. This suggests the exciting prospect that nucleic acid structures of folded RNA and DNA molecules could be obtained using phase-plate cryo-EM.

## SUPPLEMENTARY DATA

Supplementary Data are available at NAR Online.

## ACKNOWLEDGEMENT

The authors thank C. Davey for the 601–145 plasmid and advice. The authors thank W. Baumeister and FEI for organizing the Volta phase plate workshop. The authors are grateful to M. Khoshouei for plunge freezing the sample grids. The authors thank D. Rhodes, R. Henderson, S.H.W. Scheres, R.D. Borkowski and C. Boothroyd for advice and discussions. The authors also thank A. Ludwig, A. Stewart and D. Rhodes for critical reading of the manuscript. We thank R.W. Purbojati and S. Schuster for help with high-speed computing. The authors thank Gatan Inc. for their support with the K2 Summit at MPI. The structure is deposited in the EM Data Bank (accession code: EMD-8140).

## FUNDING

Singapore Ministry of Education [MOE2012-T3-1-001]; NTU Singapore [start-up grant to S.S.]; NTU Institute of Structural Biology. Funding for open access charge: [MOE2012-T3-1-001]

*Conflict of interest statement.* RD: Co-inventor in US patent US9129774 B2 “Method of using a phase plate in a transmission electron microscope”.

## REFERENCES

- Bai, X.C., McMullan, G. and Scheres, S.H. (2015) How cryo-EM is revolutionizing structural biology. *Trends Biochem. Sci.*, **40**, 49–57.
- Cheng, Y., Grigorieff, N., Penczek, P.A. and Walz, T. (2015) A primer to single-particle cryo-electron microscopy. *Cell*, **161**, 438–449.
- Nogales, E. and Scheres, S.H. (2015) Cryo-EM: A unique tool for the visualization of macromolecular complexity. *Mol. Cell* **58**, 677–689.
- Henderson, R. (1995) The potential and limitations of neutrons, electrons and X-rays for atomic resolution microscopy of unstained biological molecules. *Q. Rev. Biophys.*, **28**, 171–193.
- Baker, L.A. and Rubinstein, J.L. (2010) Radiation damage in electron cryomicroscopy. *Methods Enzymol.*, **481**, 371–388.

6. Glaeser, R.M. (2013) Invited review article: Methods for imaging weak-phase objects in electron microscopy. *Rev. Sci. Instrum.*, **84**, 111101.
7. Khoshouei, M., Radjainia, M., Phillips, A.J., Gerrard, J.A., Mitra, A.K., Plitzko, J.M., Baumeister, W. and Danev, R. (2016) Volta phase plate cryo-EM of the small protein complex Prx3. *Nat. Commun.*, **7**, 10534.
8. Kornberg, R.D. (1974) Chromatin structure: A repeating unit of histones and DNA. *Science*, **184**, 868–871.
9. Finch, J.T., Lutter, L.C., Rhodes, D., Brown, R.S., Rushton, B., Levitt, M. and Klug, A. (1977) Structure of nucleosome core particles of chromatin. *Nature*, **269**, 29–36.
10. Olins, A.L. and Olins, D.E. (1974) Spheroid chromatin units (v bodies). *Science*, **183**, 330–332.
11. Richmond, T.J., Finch, J.T., Rushton, B., Rhodes, D. and Klug, A. (1984) Structure of the nucleosome core particle at 7 Å resolution. *Nature*, **311**, 532–537.
12. Luger, K., Mader, A.W., Richmond, R.K., Sargent, D.F. and Richmond, T.J. (1997) Crystal structure of the nucleosome core particle at 2.8 Å resolution. *Nature*, **389**, 251–260.
13. Davey, C.A., Sargent, D.F., Luger, K., Maeder, A.W. and Richmond, T.J. (2002) Solvent mediated interactions in the structure of the nucleosome core particle at 1.9 Å resolution. *J. Mol. Biol.*, **319**, 1097–113.
14. Danev, R., Buijsse, B., Khoshouei, M., Plitzko, J.M. and Baumeister, W. (2014) Volta potential phase plate for in-focus phase contrast transmission electron microscopy. *Proc. Natl. Acad. Sci. U.S.A.*, **111**, 15635–15640.
15. Dyer, P.N., Edayathumangalam, R.S., White, C.L., Bao, Y., Chakravarthy, S., Muthurajan, U. M. and Luger, K. (2004) Reconstitution of nucleosome core particles from recombinant histones and DNA. *Methods Enzymol.*, **375**, 23–44.
16. Mastronarde, D.N. (2005) Automated electron microscope tomography using robust prediction of specimen movements. *J. Struct. Biol.*, **152**, 36–51.
17. Kremer, J.R., Mastronarde, D.N. and McIntosh, J.R. (1996) Computer visualization of three-dimensional image data using IMOD. *J. Struct. Biol.*, **116**, 71–76.
18. Grant, T. and Grigorieff, N. (2015) Measuring the optimal exposure for single particle cryo-EM using a 2.6 Å reconstruction of rotavirus VP6. *Elife*, **4**, e06980.
19. Ludtke, S.J., Baldwin, P.R. and Chiu, W. (1999) EMAN: semiautomated software for high-resolution single-particle reconstructions. *J. Struct. Biol.*, **128**, 82–97.
20. Scheres, S.H. (2012) RELION: implementation of a Bayesian approach to cryo-EM structure determination. *J. Struct. Biol.*, **180**, 519–530.
21. Kucukelbir, A., Sigworth, F.J. and Tagare, H.D. (2014) Quantifying the local resolution of cryo-EM density maps. *Nat. Methods*, **11**, 63–65.
22. Schneider, C.A., Rasband, W.S. and Eliceiri, K.W. (2012) NIH Image to ImageJ: 25 years of image analysis. *Nat. Methods*, **9**, 671–675.
23. Goddard, T.D., Huang, C.C. and Ferrin, T.E. (2007) Visualizing density maps with UCSF Chimera. *J. Struct. Biol.*, **157**, 281–287.
24. Adams, P.D., Afonine, P.V., Bunkóczi, G., Chen, V.B., Davis, I.W., Echols, N., Headd, J.J., Hung, L.W., Kapral, G.J. and Grosse-Kunstleve, R.W. (2010) PHENIX: A comprehensive Python-based system for macromolecular structure solution. *Acta Crystallogr. D Biol. Crystallogr.*, **66**, 213–221.
25. Lowary, P.T. and Widom, J. (1998) New DNA sequence rules for high affinity binding to histone octamer and sequence-directed nucleosome positioning. *J. Mol. Biol.*, **276**, 19–42.
26. Danev, R. and Baumeister, W. (2016) Cryo-EM single particle analysis with the Volta phase plate. *Elife*, **5**, e13046.
27. Vasudevan, D., Chua, E.Y. and Davey, C.A. (2010) Crystal structures of nucleosome core particles containing the '601' strong positioning sequence. *J. Mol. Biol.*, **403**, 1–10.
28. Yamada, K., Frouws, T.D., Angst, B., Fitzgerald, D.J., DeLuca, C., Schimmele, K., Sargent, D.F. and Richmond, T.J. (2011) Structure and mechanism of the chromatin remodelling factor ISW1a. *Nature*, **472**, 448–453.
29. Chaban, Y., Ezeokonkwo, C., Chung, W.H., Zhang, F., Kornberg, R.D., Maier-Davis, B., Lorch, Y. and Asturias, F.J. (2008) Structure of a RSC-nucleosome complex and insights into chromatin remodeling. *Nat. Struct. Mol. Biol.*, **15**, 1272–1277.
30. Song, F., Chen, P., Sun, D., Wang, M., Dong, L., Liang, D., Xu, R.M., Zhu, P. and Li, G. (2014) Cryo-EM study of the chromatin fiber reveals a double helix twisted by tetranucleosomal units. *Science*, **344**, 376–380.
31. Maskell, D.P., Renault, L., Serrao, E., Lesbats, P., Matadeen, R., Hare, S., Lindemann, D., Engelman, A.N., Costa, A. and Cherepanov, P. (2015) Structural basis for retroviral integration into nucleosomes. *Nature*, **523**, 366–369.
32. McGinty, R.K. and Tan, S. (2016) Recognition of the nucleosome by chromatin factors and enzymes. *Curr. Opin. Struct. Biol.*, **37**, 54–61.